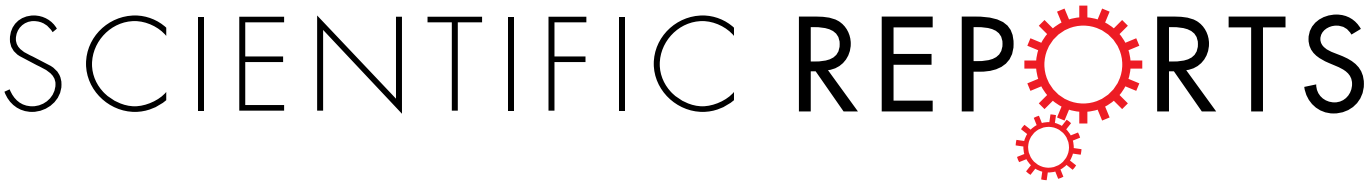

OPEN

Quantum oscillations from generic surface Fermi arcs and bulk chiral modes in Weyl semimetals

Received: 19 February 2016
Accepted: 14 March 2016
Published: 01 April 2016

Yi Zhang[1], Daniel Bulmash[1], Pavan Hosur[1], Andrew C. Potter[2] & Ashvin Vishwanath[2]

We re-examine the question of quantum oscillations from surface Fermi arcs and chiral modes in Weyl semimetals. By introducing two tools - semiclassical phase-space quantization and a numerical implementation of a layered construction of Weyl semimetals - we discover several important generalizations to previous conclusions that were implicitly tailored to the special case of identical Fermi arcs on top and bottom surfaces. We show that the phase-space quantization picture fixes an ambiguity in the previously utilized energy-time quantization approach and correctly reproduces the numerically calculated quantum oscillations for generic Weyl semimetals with distinctly curved Fermi arcs on the two surfaces. Based on these methods, we identify a 'magic' magnetic-field angle where quantum oscillations become independent of sample thickness, with striking experimental implications. We also analyze the stability of these quantum oscillations to disorder, and show that the high-field oscillations are expected to persist in samples whose thickness parametrically exceeds the quantum mean free path.

Weyl semimetals are three-dimensional quantum materials characterized by a band gap that closes at isolated points, Weyl nodes, in the Brillouin zone. Weyl nodes serve as sources of quantized monopole fluxes of $\pm 2\pi$ Berry curvature, whose sign defines a chirality $\chi = \pm 1$ for each node, and hence serves as an example of quantum topology in the absence of a band gap[1,2]. At a spatial surface, the bulk band topology produces unusual Fermi-arc surface states, whose Fermi "surface" consists of disjoint arc segments that pairwise connect surface projections of opposite chirality Weyl nodes[1–4], and have been observed in photoemission experiments[5,6] and band-structure calculations[7] on crystalline materials. Moreover, in the presence of a magnetic field, $\vec{B}$, Weyl nodes exhibit chiral Landau level (LL) modes[8] with field-independent dispersion $\varepsilon_{\chi,0} = \chi v_{\|} k_{\|}$, where $v_{\|}$, $k_{\|}$ are respectively the velocity and momentum along $\vec{B}$.

Recently, it was shown[9] that an applied magnetic field perpendicular to the surface of a Weyl semimetal drives a novel kind of cyclotron orbit in which electrons slide along a Fermi-arc on the top surface from $\chi = +1$ towards $\chi = -1$ Weyl nodes, transfers to the bulk chiral LL mode of the $\chi = -1$ node on which they propagate to the bottom surface, traverse the bottom Fermi-arc and return to the top surface via the mode with the opposite chirality. Ordinary cyclotron orbits around closed Fermi surfaces of metals are routinely studied via quantum oscillations, periodic-in-$1/B$ modulations in the density of states that appear in various thermodynamic and transport properties, and help unveil the detailed structure of the underlying Fermi surface. Ref. 9 showed that the quantized energy levels arising from these mixed surface and bulk cyclotron orbits indeed exhibit periodic quantum oscillations, whose phase exhibits a characteristic dependence on sample thickness that distinguishes them from conventional cyclotron orbits, and hence offering a direct probe of the topological connection between surface Fermi arcs and bulk Weyl bands. Experimental evidence for such quantum oscillations was recently reported in the Dirac semimetal Cd_3As_2 [10]. In addition, transport experiments were proposed based on the distinctive electronic properties of these cyclotron orbits[11].

The semiclassical quantization of these cyclotron orbits in ref. 9 was carried out through "energy-time" quantization, by demanding that the product of the energy, ε, of the electron and the semiclassical time of the orbit, t, equals an integer multiple of 2π. Noting that $t = (2L_z + 2k_0\ell_B^2)/v$, where k_0 is the k-space arc length of the Fermi arcs on the top and bottom surfaces, L_z is the sample thickness, v is the Fermi velocity, and $\ell_B = 1/\sqrt{eB}$ is the

[1]Department of Physics, Stanford University, Stanford, California 94305, USA. [2]Department of Physics, University of California, Berkeley, California 94720, USA. Correspondence and requests for materials should be addressed to Y.Z. (email: frankzhangyi@gmail.com)

magnetic length, the energy-time quantization condition states that the n^{th} quantized level crosses the chemical potential, $\tilde{\mu}$ at field $B = B_n$:

$$\frac{1}{B_n} = \frac{e}{k_0}\left[\frac{\pi v}{\tilde{\mu}}(n+\gamma) - L_z\right] \tag{1}$$

which occur periodically in $1/B$ with period $f = \frac{\pi e v}{k_0 \tilde{\mu}}$ and a thickness dependent phase offset: $\phi(L_z) = 2\pi\gamma - \frac{2\tilde{\mu}L_z}{v}$.

However, this approach leaves open a basic question: what is the overall zero of energy for $\tilde{\mu}$? This issue is experimental pertinent, as it effects the frequency, f, of the quantum oscillations. We will show that the nature choice of the energy of the bulk Weyl node corresponds to the special case, implicitly assumed in ref. 9, where the Fermi arcs on the top and bottom surfaces are identical. More generically, however, the Fermi arcs may have different shapes, and the zero of energy need not coincide with the Weyl node energy.

To generalize the results of ref. 9 to include the generic case with arbitrarily curved Fermi arcs, we adopt an alternative phase-space quantization perspective in which the integral of momentum times spatial displacement is equal to $\oint \vec{p} \cdot d\vec{r} = 2\pi(n+\gamma)$ for integer n and a constant quantum offset γ. Comparison to the energy-time quantization transparently identifies the zero of energy as where the surface arcs enclose zero k-space area using appropriate extrapolation from the chemical potential to lower energy. This method also predicts an additional thickness dependent correction to Eq. 1, which is difficult to obtain from the energy-time quantization perspective.

We also discuss the experimental consequences of our results. First, we identify a special set of 'magic' angles of the magnetic field, for which the length-dependence of the phase of the quantum oscillations drops out. We explain how this effect enables a smoking gun signature of quantum oscillations from surface Fermi arcs in recently measured thin-film devices with non-parallel surfaces[10]. Second, we examine the effects of impurities, and find that these quantum oscillations are surprisingly resilient to disorder for sufficiently strong fields. In contrast to conventional quantum oscillations, which are obscured by disorder unless the cyclotron orbit is smaller than the quantum mean free path ℓ_Q, we find that for strong fields, quantum oscillations from surface Fermi arcs and bulk chiral modes can persist in samples whose thickness substantially exceeds ℓ_Q.

Finally, we construct a tight-binding model based on a layered construction[4] of a Weyl semimetal, which enables the numerical simulation of Weyl semimetals with generic surface arcs. Using a recursive Greens function method, we numerically simulate the field dependence of the density of states in a magnetic field, and confirm the semiclassical predictions of the phase-space quantization scheme.

Results

We first revisit the semiclassical quantization of cyclotron orbits, which generically demands that the phase difference between successive Landau levels is equal to 2π. The difference in phase accumulated between two successive levels for a fixed magnetic field can be expressed either in terms of the energy step and time or the difference in the product of momentum and displacement:

$$\Delta\phi = \int \Delta\varepsilon dt = \int \frac{\Delta\varepsilon}{v_F} dr = \Delta \oint \vec{p} \cdot d\vec{r} = 2\pi \tag{2}$$

where $v_F = \frac{\partial\varepsilon}{\partial p_\perp}$ is the Fermi velocity, $p_\perp$ is the momentum perpendicular to the orbit, and the last integral is over the spatial trajectory of the semiclassical orbit. For a simple derivation via path integral, see Supplementary information, Sec. I. Importantly, Eq. 2 is expressed through the difference in energy of neighboring Landau levels but makes no reference to their absolute position. While the overall energy scale is unimportant for, e.g. spectroscopy which probes only energy differences, quantum oscillations experiments are conducted by varying B at fixed chemical potential μ, such that the periodicity of quantum oscillations depends explicitly on the "zero of energy".

Alternatively, the phase-space quantization framework offers an unambiguous reference to the energy, in which the momentum-displacement is integrated along the cyclotron orbit of constant energy contour at a specific chemical potential. In Supplementary information, we show how to reconcile these methods, however, in the mean time we proceed with the more transparent phase-space quantization approach.

For the semiclassical cyclotron orbits described in ref. 9, the phase-space quantization condition is $\oint \vec{p} \cdot d\vec{r} = \oint \vec{k} \cdot d\vec{r} - e\oint \vec{A} \cdot d\vec{r} = 2\pi(n+\gamma)$, where the integral is over the four segments of the orbit: two Fermi arcs on the surfaces and two chiral modes in the bulk parallel to the magnetic field, as illustrated in Fig. 1. There may exist additional phase contributions at the turning points connecting the surface and bulk orbits, which are presumably constant for large enough L_z and can be absorbed into the constant γ. Throughout, we choose the convention that chemical potential, μ, is measured from the energy of the Weyl nodes in the bulk.

For the Fermi arcs, $\int \vec{p} \cdot d\vec{r} = e\Phi_z$, where Φ_z is the magnetic flux contained within the real-space orbit of area S_R in the $x-y$ plane[12]. The semiclassical equations of motion imply

$$\Phi_z = B_z S_R = B_z S_k \ell_B^4 = \frac{S_k}{e^2 B_z} \tag{3}$$

where S_k is the k-space area enclosed by the two Fermi arcs combined and B_z is the $\hat{z}$ component of the magnetic field $\vec{B}$. On the other hand, the chiral modes in the bulk are parallel to the magnetic field, so $\int \vec{A} \cdot d\vec{r} = 0$ and:

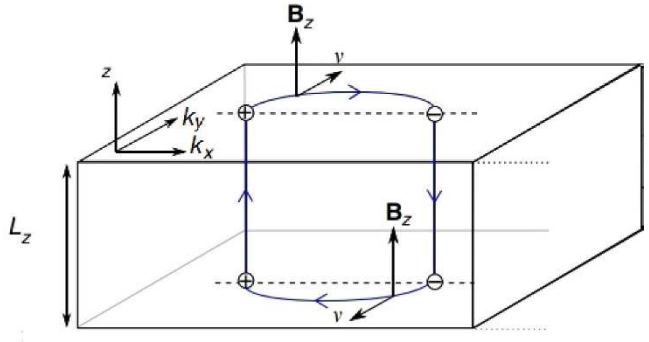

Figure 1. Schematic plot of a semiclassical orbit of a Weyl semimetal slab in a perpendicular magnetic field. The electrons traverse the Fermi arc on the top surface, travel through the one-dimensional chiral mode parallel to the magnetic field in the bulk, traverse the corresponding Fermi arc on the bottom surface, and then return along the opposite chiral mode through the bulk. Note that the real-space orbit in the $x-y$ plane is rotated by 90°.

$$\int \vec{p}\cdot d\vec{r} = \int \vec{k}\cdot d\vec{r} = L_z \sec\theta\left(\vec{k}_W\cdot\hat{B} + 2\frac{\mu}{v_\parallel}\right) \tag{4}$$

where θ is the tilting angle of $\vec{B}$ from the surface normal, $\vec{k}_W$ is the wave vector from + to − chirality Weyl nodes, and $\pm\frac{\mu}{v_\parallel}$ are the Fermi wave vectors of their respective chiral modes with velocity $v_\parallel$ parallel to $\vec{B}$, at chemical potential μ. Adding the contributions, phase-space quantization implies that quantum oscillations occur at fields:

$$\frac{1}{B_n} = \frac{e}{S_k}\left[2\pi(n+\gamma)\cos\theta - L_z\left(\vec{k}_W\cdot\hat{B} + \frac{2\mu}{v_\parallel}\right)\right] \tag{5}$$

Eq. 5 is the main result of this paper.

Discussion

Comparison with and generalization to previous conclusions. When μ is close to the Weyl nodes and the Fermi velocity v_s is approximately constant along the surface Fermi arcs, we can expand $S_k = S_{k,0} + k_0^T\mu/v_s$, where $S_{k,0}$ and k_0^T are the enclosed k-space area and total length of the combination of the two Fermi arcs from both surfaces for μ at the Weyl nodes. The frequency of the quantum oscillations $f = 1/\Delta\left(\frac{1}{B}\right)$ is

$$\begin{aligned} f &= S_k/2\pi e = (S_{k,0} + k_0^T\mu/v_s)/2\pi e \\ &= k_0^T(\mu_0+\mu)/2\pi e v_s \end{aligned} \tag{6}$$

where $\mu_0 = S_{k,0}v_s/k_0^T$. We see that our results reduce to those of ref. 9, under the special conditions: $S_k(\mu=0)=0$, $\vec{k}_W\cdot\hat{B}=0$, and $v_s = v_\parallel$. However, the phase-space quantization method reveals two important generalizations:

(1) The $\tilde{\mu}$ defined in Eq. 1 is generically not measured from the energy of the bulk Weyl nodes. In particular, if we require that μ is measured from the Weyl nodes, Eq. 1 should be modified by an offset $\tilde{\mu} = \mu + \mu_0$. This reconciles the quantum oscillations from phase-space quantization and energy-time quantization: the contribution from the area $S_{k,0}$ enclosed by the Fermi arcs at $\mu=0$ is reflected in μ_0 while the contribution from the area change $S_k - S_{k,0} = k_0^T\mu/v_s$ is reflected in μ. For cases where the area $S_{k,0}$ is large in comparison with the area change, the inclusion of μ_0 is necessary for the correct interpretation of the quantum oscillations.
It is natural that μ_0 should depend only on linearized Fermi-surface properties such as the area enclosed and the Fermi velocity, as the quantum oscillations generically encode only these low-energy universal features. We note that since v_s can in principle depend on chemical potential, μ, so does μ_0 as defined above. For a quadratic surface dispersion, $-\mu_0$ can be interpreted as the energy (relative to the bulk Weyl nodes) at which the surface arcs enclose zero area perpendicular to the magnetic field. More generally, as we show in Supplementary information, the appropriate way to reconcile energy-time quantization is to set the zero of energy $-\mu_0$ at $\mu_0 = \frac{S_k}{\partial S_k/\partial\mu}$, as the zero-area energy linearly extrapolated using the Fermi-surface property $\frac{\partial S_k}{\partial\mu} \approx \frac{k_0^T}{v_s}$.

(2) The thickness of the Weyl semimetal slab L_z contributes to the quantum oscillations through the phase offset of $\phi(L_z) = \left(\vec{k}_W\cdot\hat{B} + \frac{2\mu}{v_\parallel}\right)L_z\sec\theta$, which shifts the $1/B$ positions of the quantum oscillation peaks. Comparing to ref. 9, we see that the thickness dependent phase receives a contribution not only from the time $t_{\text{bulk}} = \frac{L_z\ \sec\ \theta}{v_\parallel}$ taken to traverse the bulk via the chiral mode, but also from the momentum-space separation

of the Weyl nodes projected onto $\vec{B}$. Interestingly, for fixed chemical potential μ, there exists a special cone of angles of $\vec{B}$, defined by: $\vec{k}_W \cdot \hat{B} = -\frac{2\mu}{v_\parallel}$, for which the phase vanishes, $\phi(L_z) = 0$, for all L_z, such that the oscillations become independent of sample thickness.

Experimental consequences. The new features revealed by the phase-space quantization treatment have several implications for experiments. As an example, the angle and thickness dependence of $\phi(L_z)$, observable by tracking individual quantum oscillation peaks as a function of field orientation, can be used to quantitatively determine the k-space separation of the Weyl nodes from quantum oscillation measurements, which can be challenging to accurately extract from other probes such as photoemission.

Magic Angles. Moreover, the existence of a special set of angles for which the quantum oscillations become independent of sample thickness enables the following test: In recent experiments[10], Moll *et al.* observed surface state oscillations in the Dirac semimetal Cd_3As_2 in thin film devices with parallel surfaces, which were absent in triangular devices with non-parallel top and bottom surfaces. The absence of oscillations in the latter triangular samples can be attributed to the destructive interference of orbits with different L_z, due to the variation of device thickness along the triangle. The above computations predict that this geometric interference effect would be quenched for fields along the set of angles for which $\phi(L_z) = 0$, resulting in a reemergence of quantum oscillations. In contrast to the negative signature of not observing quantum oscillations in a triangular device, which could potentially arise from other extrinsic effects, such an observation would provide a clear positive signature of the non-local nature of the Weyl orbits. We note that observing this effect requires the field angle to be controlled to angular precision $\delta\theta \lesssim 1/k_W L_z$, which may require thin devices.

Disorder and Thickness Dependence. As a final application, the phase-space quantization formulation above naturally reveals the effect of bulk disorder on dephasing the quantum oscillations associated with Weyl orbits. See Supplementary information, Sec. IV for a detailed discussion of disorder effects. For conventional magnetic orbits, any scattering from impurities strongly suppresses quantum oscillations, requiring $B \gg k_F/\ell_Q$ where ℓ_Q is the quantum mean-free path (distinct from the transport mean-free path, ℓ_{tr}, which only includes large-momentum transfer scattering) and k_F is the Fermi wave vector. As the surface-arc portion of the Weyl orbits is locally identical to conventional cyclotron motion, observing oscillations in the presence of disorder requires: $B \gg k_0^T/\ell_Q$. Naively, phase coherence along the bulk part similarly requires samples thinner than the quantum mean-free path, $L_z \gg \ell_Q$, a potentially stringent condition since while typical Weyl materials have large ℓ_{tr}, ℓ_Q is typically much shorter[13]. However, the chiral nature of the bulk orbit along with the spatially correlated nature of disorder in low-density semimetals makes the bulk portion of the orbit more resilient to disorder effects.

Namely, for an electron traveling along a bulk chiral LL, a random potential $V(\vec{r})$, produces a local shift in the wave vector: $\delta k_\parallel(\vec{r}) = -\tilde{V}(\vec{r}_\perp, z)/v_\parallel$, where $\tilde{V}$ is the matrix element of the disorder potential in the chiral mode localized within $\approx \ell_B$ of transverse position $\vec{r}_\perp$ in the xy-plane. The total phase accumulated in this fashion is given by: $\delta\phi = \int_0^{L_z} dz\,(\delta k_\parallel(\vec{r}_\perp, z) - \delta k_\parallel(\vec{r}_\perp + \vec{d}, z))$, where the first term represents the random phase acquired traveling from bottom to top surface along the + chiral mode, and the second represents that of the return journey on the counter-propagating chiral mode of the opposite Weyl node. Between these two bulk legs of the orbit, the electron travels a spatial distance $d \approx k_0^T \ell_B^2$ as it slides along the top surface Fermi arc. The typical disorder for low-density Weyl semimetals is poorly screened Coulomb impurities, which produce a potential that is spatially correlated over characteristic length scale $\xi \approx \sqrt{\frac{\ell_{tr}}{\ell_Q}} k_F^{-1} \gg k_F^{-1}$. For low-field, $d \gg \xi$, the two bulk legs of the orbit sample uncorrelated V, and dephasing indeed kills the quantum oscillations for $L_z > \ell_B$. However, for higher fields $eB \gg k_0^T/\xi$, $d \ll \xi$ and the top-to-bottom and bottom-to-top legs accumulate nearly canceling random phases, which leads to the much weaker requirement on sample thickness, $L_z < \left(\frac{\xi}{d}\right)^2 \ell_Q \gg \ell_Q$. For example, in Cd_3As_2, we estimate that the high-field regime is obtained for relatively low fields on the order of a few Tesla, in reasonable agreement with the observed field-scale at which surface-state oscillations onset in recent experiments[10].

In conclusion, we have compared quantum oscillations with respect to the inverse magnetic field $1/B$ or chemical potential μ. The accurate definition of chemical potential and its reference point is vital for correctly converting between and reconciling different semi-classical quantization perspectives. For the quantum oscillations from the surface Fermi arcs and bulk chiral modes in Weyl semimetals, the general reference point of μ does not necessarily coincide with the Weyl points in the bulk. We derived the quantum oscillations using phase-space quantization conditions and proposed essential generalizations to previous conclusions and experimental consequences for generic Weyl semimetals. In the next section, we verify our claims numerically following the layered prescription.

Methods

To verify the semiclassical predictions from the phase-space quantization approach we study a simple lattice model of Weyl semimetal following the layered prescription in ref. 4 and numerically calculate the density of states $\rho(\mu, \vec{B})$ in a slab geometry. In the absence of the magnetic field, the Weyl semimetal is characterized by the following Hamiltonian:

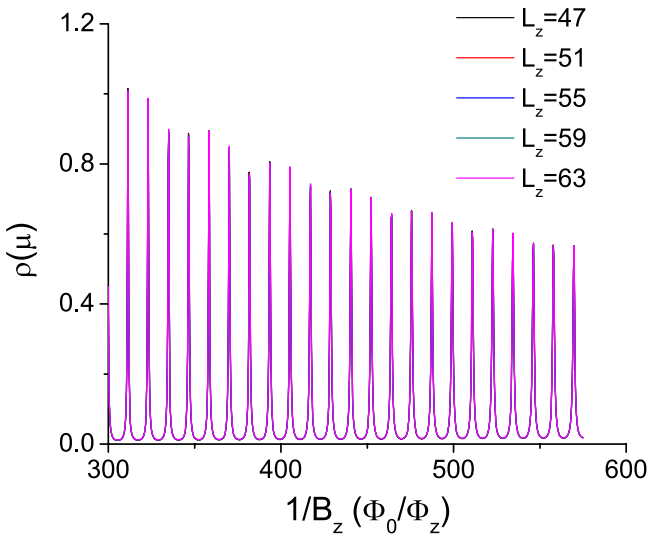

Figure 2. The density of states $\rho(\mu)$ versus the inverse magnetic field $1/B_z$ (in unit of Φ_0/Φ_z) for a Weyl semimetal slab of various thickness L_z shows clear quantum oscillations. The chemical potential $\mu = 0$ is at the Weyl nodes. The characteristic quantum oscillation period is $\Delta(\Phi_0/\Phi_z) = 11.74$.

$$H_{\vec{k}} = \sum_{z=1}^{L_z} (-1)^{z-1} \varepsilon_{\vec{k}} c^{\dagger}_{\vec{k},z} c_{\vec{k},z} + \sum_{z=1}^{L_z-1} h_{\vec{k},z} c^{\dagger}_{\vec{k},z+1} c_{\vec{k},z} + \text{H.c.} \tag{7}$$

where $\vec{k} = (k_x, k_y)$ and the total number of layers L_z is odd so that the Fermi arcs on the top and bottom surfaces can be different[4]. We consider an in-plane dispersion $\varepsilon_{\vec{k}} = -2\cos k_x - 2\cos k_y + \varepsilon_0$ that represents nearest-neighbor hopping of amplitude -1 and an on-site energy of ε_0. $h_{\vec{k},z}$ represents nearest-neighbor interlayer hopping with $h_{\vec{k},z} = -t \sin k_y - t_0$ if z is odd and $h_{\vec{k},z} = t\lambda \sin k_y + t_0$ if z is even. We choose $\lambda > 1$, which ensures $|h_{\vec{k},2}| > |h_{\vec{k},1}|$ if $k_y > 0$ and vice versa. This model generates two Weyl nodes at $(\pm k_x^0, 0, 0)$ where k_x^0 is the in-plane Fermi wave vector of $\varepsilon_{\vec{k}}$ along the $\hat{x}$ direction. By definition $\vec{k}_W = 2k_x^0\hat{x}$. The surface Fermi arcs and the bulk chiral modes following the Weyl nodes are schematically consistent with the geometry in Fig. 1.

In the presence of a magnetic field $\vec{B}$, the translation symmetry in the $\hat{y}$ direction is preserved in the Landau gauge $\vec{A} = (0, \Phi_z x - \Phi_x z, -\Phi_y x)$, where Φ_i is the flux per plaquette perpendicular to the $\hat{i}$ direction in units of the magnetic flux quantum, $\Phi_0 = \frac{h}{e}$, $i = x, y, z$. The Hamiltonian becomes:

$$\begin{aligned} H_{k_y} &= \sum_{x,z} h_{\pi_y(x,z+1/2),z} (e^{-i\Phi_y x} c^{\dagger}_{x,z+1} c_{x,z} + \text{h.c.}) \\ &\quad - (-1)^z \left[(\varepsilon_0 - 2\cos \pi_y(x,z)) c^{\dagger}_{x,z} c_{x,z} - c^{\dagger}_{x\pm1,z} c_{x,z} \right] \end{aligned} \tag{8}$$

where $\pi_y(x,z) = k_y - A_y(x,z)$.

The properties of this Hamiltonian such as the density of states $\rho(\mu) = -\frac{1}{\pi L_x L_z} \sum_{x,z} \text{Im}\, G(x, z; x, z; \mu)$ at the chemical potential μ can be calculated with the recursive Green's function method where the real space degrees of freedom in the $\hat{x}$ direction are treated recursively[14–16]. For an incommensurate flux Φ, physical properties of H_{k_y} between different choices of k_y are equivalent in the thermodynamic limit[15,16] and the summation over k_y can be neglected.

We choose parameters $\varepsilon_0 = 3.0$, $t = 1.0$, $t_0 = 2.0$, $\lambda = 2.0$, and a small imaginary part $\delta = 0.001$ in addition to the chemical potential μ as the level broadening. In this model, although the chemical potential is at the Weyl nodes, the Fermi arcs enclose a k-space area of 8.515% of the surface Brillouin zone. We first consider a magnetic field purely in the $\hat{z}$ direction. Eq. 1 would predict no quantum oscillations if one assumed $\tilde{\mu} = 0$, while Eq. 5 predicts quantum oscillations with a period $\Delta(\Phi_0/\Phi_z) = 11.74$. The numerical results of the density of states $\rho(\mu)$ versus the inverse magnetic field $1/B$ and various slab thickness L_z, shown in Fig. 2, show clear signatures of quantum oscillations whose period is in quantitative agreement with our formula.

To verify that the semiclassical orbit contains components in the bulk as well as on both of the top and bottom surfaces, we calculate the local density of states distribution $\rho(x, z, \mu) = -\frac{1}{\pi} \text{Im}\, G(x, z; x, z; \mu)$ in the $x - z$ plane with the x coordinate replaced by $x + k_y/\Phi_z$. The result for $\Phi_0/\Phi_z = 311.40$, $\mu = 0$ and $L_z = 103$ is shown in Fig. 3. The Fermi arcs are at $k_y > 0$ and $k_y < 0$ for the top and bottom surfaces as well as the chiral modes in the bulk are clearly visible.

In addition, Eq. 5 suggests that the thickness of the slab L_z changes the phase of the quantum oscillations, and thus the actual locations of the $\rho(\mu)$ peaks in Φ_0/Φ_z. For a magnetic field in the $\hat{z}$ direction and $\mu = 0$, $\vec{k}_W \cdot \hat{B} = 0$,

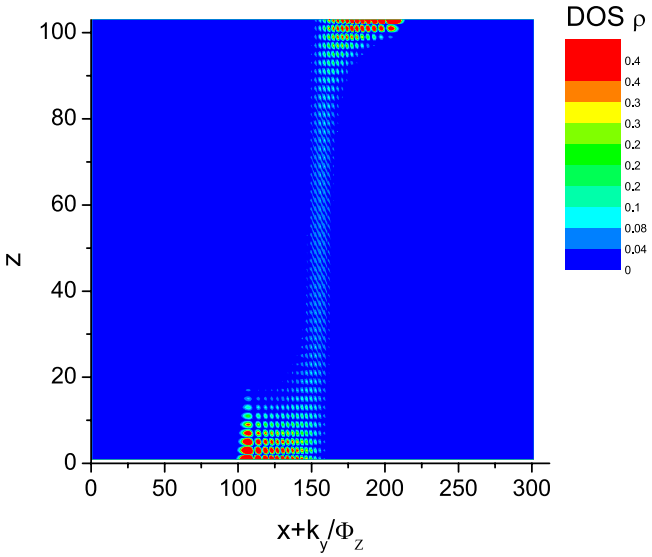

Figure 3. The local density of states distribution in the $x-z$ plane at $\Phi_0/\Phi_z = 311.40$, $\mu = 0$ and $L_z = 103$ is consistent with the cyclotron orbit illustrated in Fig. 1 and clearly consists of components from the Fermi arcs on both Fermi surfaces and chiral LL modes in the bulk.

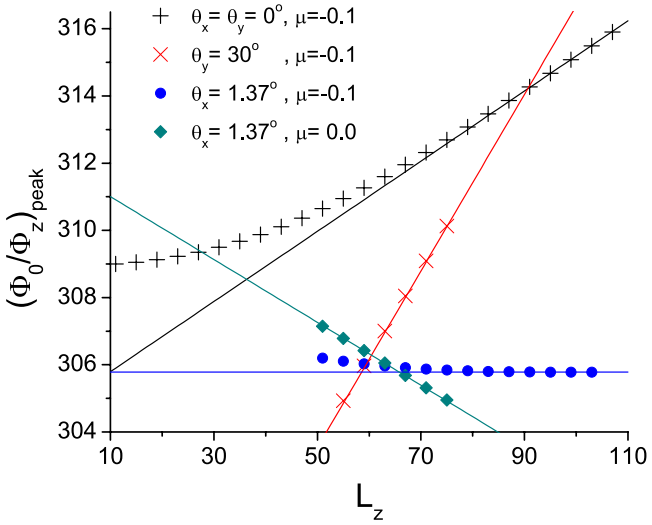

Figure 4. Symbols mark the location of one of the density of states peaks as a function of the slab thickness L_z at different chemical potential μ and magnetic field tilting angle θ_y or θ_x. The lines are the asymptotic expression in the large L_z limit derived from the positions of and the Fermi velocity around the Weyl nodes in the bulk: $\left(\frac{\Phi_0}{\Phi_z}\right)_{\text{peak}} = \text{const.} + L_z \cdot \frac{-\mu}{2\pi t_0} \cdot \Delta\left(\frac{\Phi_0}{\Phi_z}\right)$ for a magnetic field in the $\hat{z}$ direction, and refer to Supplementary information for the expressions in the presence of a tilted magnetic field. While the peak positions typically show strong L_z dependence, notably, for particular 'magic' angles (blue circles), the peak positions asymptotically become nearly independent of sample thickness.

we expect no L_z dependence, which is confirmed in Fig. 2. For a finite μ and a field in the $\hat{z}$ direction, however, the shift $\delta(1/B)$ of the peak positions is given by

$$\delta\left(\frac{\Phi_0}{\Phi_z}\right) = -\frac{\mu}{v_z}\frac{2\delta L_z}{2\pi} \cdot \Delta\left(\frac{\Phi_0}{\Phi_z}\right) = -\delta L_z \cdot \frac{\mu}{2\pi t_0} \cdot \Delta\left(\frac{\Phi_0}{\Phi_z}\right) \tag{9}$$

where $\Delta\left(\frac{\Phi_0}{\Phi_z}\right)$ is the period of the quantum oscillations. We numerically observe this shift in the locations of the quantum oscillation peaks at $\mu = -0.1$ in Fig. 4, where the location of one of the peaks is tracked as L_z is varied. The deviation from Eq. 9 at small L_z is due to the finite extent of the edge states (Fig. 3). At relatively large L_z where the physics in the center of the slab can be approximately treated as in the bulk, Eq. 9 gives an accurate description

of the L_z dependence of the quantum oscillation phenomena. The above conclusions also hold true for a magnetic field that is tilted in the $\hat{y}$ direction, e.g. $\vec{B} = B_z(\hat{z} + \hat{y}\ \tan\theta_y)$, where only the L_z coefficient is modified, see Fig. 4.

In comparison, the magnetic field tilted in the $\hat{x}$ direction gives qualitatively different behavior, since $\vec{k}_W \cdot \hat{B} \neq 0 \text{along} \vec{B} = B_z(\hat{z} + \hat{x}\ \tan\theta_x)$. First, there exists L_z dependence $\delta\left(\frac{\Phi_0}{\Phi_z}\right) = -\delta L_z \cdot k_x^0\ \tan\ \theta_x \cdot \Delta\left(\frac{\Phi_0}{\Phi_z}\right)/\pi$ for chemical potential $\mu = 0$ at the energy of the Weyl nodes. Interestingly, for a given chemical potential μ, such L_z dependence vanishes at a special tilting angle $\theta_x^{(0)}$, which satisfies

$$\tan\theta_x^{(0)} = -\frac{\mu}{t_0}[4(k_x^0)^2 - \mu^2/\sin^2(k_x^0)]^{-1/2} \tag{10}$$

Numerical results for $\mu = 0$ and $\mu = -0.1$ confirm these expectations at tilting angle $\theta_x^{(0)} \approx 0.024$ as in Eq. 10 for $\mu = -0.1$ (Fig. 4). Derivations and further discussion on the L_z dependence of the peak positions in a tilted magnetic field $\vec{B}$ are in Supplementary information.

References

1. Wan, X., Turner, A. M., Vishwanath, A. & Savrasov, S. Y. Topological semimetal and Fermi-arc surface states in the electronic structure of pyrochlore iridates. *Phys. Rev. B* **83,** 205101 (2011).
2. Turner, A. M. & Vishwanath, A. Beyond Band Insulators: Topology of Semi-metals and Interacting Phases. eprint-arXiv:1301.0330 (2013).
3. Haldane, F. D. M. Attachment of Surface "Fermi Arcs" to the Bulk Fermi Surface: "Fermi-Level Plumbing" in Topological Metals. eprint-arXiv:1401.0529 (2014).
4. Hosur, P. Friedel oscillations due to Fermi arcs in Weyl semimetals. *Phys. Rev. B* **86,** 195102 (2012).
5. Xu, S. Y. *et al.* Discovery of a Weyl fermion semimetal and topological Fermi arcs. *Science* **349,** 613–617 (2015).
6. Lv, B. Q. *et al.* Experimental Discovery of Weyl Semimetal TaAs. *Phys. Rev. X* **5,** 031013 (2015).
7. Weng, H. M., Fang, C., Fang, Z., Bernevig, B. A. & Dai, X. Weyl Semimetal Phase in Noncentrosymmetric Transition-Metal Monophosphides. *Physical Review X* **5,** 011029 (2015), Huang, S. M. *et al.* A Weyl Fermion semimetal with surface Fermi arcs in the transition metal monopnictide TaAs class. *Nature Communications* **6**, 7373 (2015).
8. Nielsen, H. B. & Ninomiya, M. The Adler-Bell-Jackiw anomaly and Weyl fermions in a crystal, *Physics Letters* **130B,** 6, 389–396 (1983).
9. Potter, A. C., Kimchi, I. & Vishwanath, A. Quantum oscillations from surface Fermi arcs in Weyl and Dirac semimetals. *Nature Communications* **5,** 5161(2014).
10. Moll, P. J. W. *et al.* Chirality transfer dynamics in quantum orbits in the Dirac semi-metal Cd_3As_2. eprint-arXiv:1505.02817 (2015).
11. Baum, Y., Berg, E., Parameswaran, S. A. & Stern, A. Current at a Distance and Resonant Transparency in Weyl Semimetals. *Phys. Rev. X* **5,** 041046 (2015).
12. Onsager, L. Interpretation of the de Haas-van Alphen effect. *Phil. Mag.* **43,** 1006–1008 (1952), Lifshitz, I. M. & Kosevich, A. M. Sov. *Phys. JETP* **2**, 636 (1956).
13. Liang, T. *et al.* Ultrahigh mobility and giant magnetoresistance in the Dirac semimetal Cd_3As_2. *Nature Materials* **14,** 280–284 (2015).
14. Croy, A., Roemer, R. A. & Schreiber, M. *Lecture Notes in Computational Science and Engineerings* 203 (Springer 2006).
15. Zhang, Y., Maharaj, A. V. & Kivelson, S. A. Disruption of quantum oscillations by an incommensurate charge density wave. *Physical Review B* **91,** 085105 (2015).
16. Zhang, Y., Bulmash, D., Maharaj, A. V., Jian, C. M. & Kivelson, S. A. The almost mobility edge in the almost Mathieu equation. eprint-arXiv:1504.05205.

Acknowledgements

We acknowledge insightful discussions with Itamar Kimchi, and Steven A. Kivelson. YZ was supported by the NSF under Grant No. DMR-1265593. DB was supported by the NSF under Grant No. DGE-114747. PH was supported by the David and Lucile Packard Foundation. AP was supported by the Gordon and Betty Moore Foundation's EPiQS Initiative through Grant GBMF4307. AV was supported by ARO MURI program W911NF-12-1-0461.

Author Contributions

Y.Z. studied the semiclassical quantization conditions and performed the numerical studies of the lattice models. D.B., P.H. and Y.Z. analyzed the the quantum oscillation from energy-time quantization conditions. A.P., A.V. and Y.Z. proposed the experimental consequences and disorder effects. All authors contributed to and reviewed the manuscript.

Additional Information

Supplementary information accompanies this paper at http://www.nature.com/srep

Competing financial interests: The authors declare no competing financial interests.

How to cite this article: Zhang, Y. *et al.* Quantum oscillations from generic surface Fermi arcs and bulk chiral modes in Weyl semimetals. *Sci. Rep.* **6**, 23741; doi: 10.1038/srep23741 (2016).